RSC Advances

PAPER

View Article Online
View Journal | View Issue

Cite this: *RSC Adv.*, 2017, **7**, 581

Surfactant-assisted synthesis of hierarchical NH_2-MIL-125 for the removal of organic dyes

Shen Hu,[a] Min Liu,[a] Keyan Li,[a] Chunshan Song,*[ab] Guoliang Zhang[c] and Xinwen Guo*[a]

Received 24th October 2016
Accepted 14th November 2016

DOI: 10.1039/c6ra25745c

www.rsc.org/advances

NH_2-MIL-125(Ti) is a promising microporous MOF material which has potential applications in photocatalytic and catalytic oxidation reactions. In this work, a facile surfactant assistant synthetic method was employed to obtain hierarchical NH_2-MIL-125 with the mesoporosity for photocatalytic degradation of organic dyes. The as-prepared NH_2-MIL-125 showed excellent dye removal efficiency due to the combination of improved adsorption and photodegradation. Compared with the microporous NH_2-MIL-125, the adsorption capacity of organic dyes increased 28% on hierarchical NH_2-MIL-125 and the photodegradation rate approximately increased 2.4 times according to the structure with abundant mesopores and macropores. The morphology of hierarchical NH_2-MIL-125 can also be modulated from tetragonal plates to truncated bipyramids and octahedrons, and the obtained catalyst shows similar enhanced photodegradation performance.

Introduction

In recent years, much dye-containing wastewater has been produced in the textiles, paper, and printing industries which has caused serious environmental issues because of compounds high toxicity, solubility, persistence and carcinogenicity.[1] Various techniques have been explored to remove the hazardous chemical compounds from wastewater in the past several decades including adsorption, photo-degradation, electrolysis, and biodegradation.[2] Adsorption and photo-degradation are considered to be the most competitive techniques among all of these applications due to the advantages of low cost, high efficiency, and environment-friendliness.[3] The dye removal efficiency by adsorbents mainly relies on the pore volume and specific surface areas of adsorbents, while the photo-degradation is closely related to the photocatalytic activities of catalysts.[4] It is a promising way to combine the adsorption and photodegradation method to enhance the dye removal efficiency.

Metal organic frameworks (MOFs), with the inherent large surface areas, uniform but tunable cavities, and tailorable physicochemical properties have enabled them to exhibit a variety of potential applications, such as gas adsorption and storage, separation, drug delivery, and catalysis.[5] The high surface area and large pore volume make MOFs a good adsorbent for water purification.[6] Significantly, the applications of MOFs in photocatalysis and degradation of model organic pollutants have attracted researchers' attention.[7] A lot of MOFs have been studied as photocatalysts. Several kinds of Fe(III)-based MOFs showed the photocatalytic activity for visible light degradation of organic pollutants in aqueous solution.[8] Lang and coworkers reported that the Zn(II) and Cd(II) MOFs constructed with diimidazole and dicarboxylatemixed ligands showed good photocatalytic performance and recyclability.[9] Some bimetallic MOFs were applied as catalysts for the removal of Bismarck brown as a diazo dye under mild conditions.[10] The porous MOFs with good adsorption performance show excellent organic pollutant removal ability cooperating with the photocatalytic activity.

NH_2-MIL-125(Ti), an amine-functionalized Ti-based metal organic framework structure, is a promising photocatalyst due to its photocatalytic and catalytic oxidation performance.[11] Many researchers focused on NH_2-MIL-125 and developed various strategies to improve the photocatalytic activity. Zhu *et al.* prepared Ni-doped NH_2-MIL-125(Ti) catalyst and used them for the photocatalytic aerobic oxidation of aromatic alcohols upon visible light irradiation.[12] Wang and coworkers synthesized core–shell In_2S_3@MIL-125(Ti) hybrid for the removal of tetracycline from wastewater by integrated adsorption and visible-light-driven photocatalysis.[4] Graphitic carbon nitride (g-C_3N_4) and reduced graphene oxide (rGO) were also composited with Ti-MOF to obtain improved photocatalytic activity.[13] Carboni *et al.* reviewed the photosensitivity of titanium and zirconium MOFs, and gave some perspectives and

[a]*State Key Laboratory of Fine Chemicals, PSU-DUT Joint Center for Energy Research, School of Chemical Engineering, Dalian University of Technology, Dalian 116024, P. R. China. E-mail: guoxw@dlut.edu.cn; Fax: +86-0411-84986134; Tel: +86-0411-84986133*

[b]*EMS Energy Institute, PSU-DUT Joint Center for Energy Research and Department of Energy & Mineral Engineering, Pennsylvania State University, University Park, Pennsylvania 16802, USA. E-mail: csong@psu.edu; Fax: +1-814-865-3573; Tel: +1-814-863-4466*

[c]*College of Biological and Environmental Engineering, Zhejiang University of Technology, Hangzhou 310014, P. R. China*

opportunities of Zr and Ti MOFs for photosynthesis and photocatalysis.[14] NH_2-MIL-125(Ti) has two types of cages corresponding to the octahedral (~12.55 Å) and tetrahedral (~6.13 Å) vacancies of a cc packing with triangular narrow windows (5–7 Å). However the size of most organic dyes is over 2 nm which makes the adsorption and diffusion of the organic dyes on the catalysts difficult. Thus, preparing MOFs with more flexible porous structure could have more excellent performance in organic dyes removal by combining the adsorption and photodegradation processes. Several strategies were applied to synthesize mesoporous MOFs like surfactant-directed method, *in situ* transformation methodology, self-assembly template strategy and kinetically controlled perturbation process.[15] Hicks and coworkers used a chelating agent-free, vapor-assisted crystallization method to synthesize hierarchical microporous/mesoporous MIL-125(Ti) and the obtained catalyst showed a marked enhancement in activity in the oxidation of an aromatic sulfur compound.[16] Compared with MIL-125, NH_2-MIL-125 shows an improved absorption in the visible light region by substituting the organic linker H_2-BDC by NH_2-BDC.[11] It can be predicted that hierarchical NH_2-MIL-125 will have an excellent adsorption performance and photocatalytic activity to remove organic dyes.

Cetyltrimethyl ammonium bromide (CTAB), as a normal surfactant, is widely used as a soft template to form mesoporous structure in the preparation of a lot of materials.[17] CTAB was applied to integrate mesoporous SiO_2 shell with magnetic particles to form core–shell composite microspheres.[18] Hydrothermally stable mesoporous aluminosilicates with ordered hexagonal structure were synthesized using tetraethylammonium hydroxide (TEAOH) and CTAB as co-templates and strongly acidity and super stability were obtained.[19] CTAB was also applied to synthesize mesoporous films for more applications.[20] The surfactant was recently employed to MOF synthesis and caused changes of morphology and porosity.[21]

Herein, we report a simple method to synthesize hierarchical NH_2-MIL-125 with substantial mesopores and macropores by employing surfactant CTAB as an additive. When the obtained hierarchical NH_2-MIL-125 was used for photocatalytic degradation of Rhodamine B (RhB), they showed increased dye removal on account of the conjugation of improved adsorption and photodegradation due to the hierarchical pores. The photodegradation performance maintains well even after four repeated cycles of regeneration. At the same time, hierarchical NH_2-MIL-125 with different morphologies was prepared using the same CTAB assisted method and showed similar enhanced photodegradation performance. This CTAB assisted synthetic strategy is suitable for more systems to obtain hierarchical MOFs for more applications.

Experimental

Materials and chemicals

2-Amino-1,4-benzenedicarboxylic acid (NH_2-BDC) and titanium isopropoxide ($C_{12}H_{28}O_4Ti$, TOPT) were purchased from Aldrich. Cetyltrimethyl ammonium bromide (CTAB) was achieved from Tianjin Guangfu Fine Chemical Reagent Co., Ltd. (China). *N*,*N*-Dimethylformamide (DMF), and methanol (CH_3OH) were obtained from Shanghai Chemical Reagent Inc. of the Chinese Medicine Group. All chemicals were used as received without further purification.

Synthesis of NH_2-MIL-125(Ti) crystals

The synthesis of NH_2-MIL-125(Ti) crystals was accomplished through a solvothermal route in a DMF-methanol mixed solvent with NH_2-BDC and TPOT as the organic linker and metal source using different amount of CTAB as an additive. In a typical synthesis, NH_2-BDC (0.56 g, 3.1 mmol) was dissolved in 40 mL of DMF and methanol mixed solvent ($V_{DMF}/V_{methanol} = 9:1$). Then specific amount of CTAB was added into the NH_2-BDC solution. In detail, the CTAB/NH_2-BDC molar ratios were varied from 0.5 to 2.0. After dissolving, TPOT (0.6 mL, 2.0 mmol) was dropped into the mixture and continued stirring for a sufficient time. Then the mixture was moved to a 100 mL Teflon-lined steel autoclave and placed in an oven at 150 °C for 24 hours under static conditions. After cooling, the yellow solid product was washed for three times with DMF and twice with methanol to remove the remaining metal and organic parts. After drying overnight in a vacuum oven at 60 °C, the samples were calcined at 200 °C for 6 hours to remove CTAB and the free solvents.

In our previous work, NH_2-MIL-125 with different morphologies from tetragon to octahedron were synthesized by modulating the concentration of the reactant.[22] We applied the morphology-controlled method to this CTAB assisted synthesis system. In detail, the concentration of CTAB was maintained as same as the maximum condition of last section.

Characterization methods

Powder X-ray diffraction (XRD) patterns were recorded on a Rigaku SmartLab(9) diffractometer, using Cu Kα radiation. The size and morphology of samples were characterized using field-emission scanning electron microscopy (NOVA NanoSEM 450). Transmission electron microscopy (TEM) images were taken using a Tecnai G2 20 S-twin instrument (FEI Company) with an acceleration voltage of 200 kV. Thermogravimetric analysis (TGA) was performed on a SDT Q600 (TA Instruments, USA) in the temperature range of 25–650 °C under air atmosphere at a heating rate of 10 °C min^{-1}. Ar adsorption/desorption isotherms were recorded at 87 K on a Quantachrom Autosorb-iQ instrument. Prior to measurement, samples were outgassed at 130 °C overnight. Diffuse reflectance UV-Vis spectroscopy (DR/UV-Vis) experiments were performed using a JASCO 550 spectrophotometer.

Photocatalytic experiment

The photocatalytic activities of different samples were tested by photocatalytic degradation of RhB aqueous solution under visible light irradiation using a 500 W Xe arc lamp with a 420 nm cutoff filter as the light source. Typically, 20 mg of photocatalyst sample was added into 50 mL of 100 mg L^{-1} RhB aqueous solution in a home-made cylindrical Pyrex vessel reactor. The suspension was magnetically stirred in the dark for 60 min to establish the adsorption–desorption equilibrium and

illuminated for 120 min to photodegrade RhB. During this process, samples were collected *via* filtrating by 0.22 μm PTFE syringe filters at predetermined time intervals. The concentration of RhB left in the supernatant solution was determined by using a Jasco V-570 UV/VIS/NIR spectrophotometer at its maximum absorption wavelength of 554 nm.

Results and discussion

Characterization

Fig. 1 shows the SEM and TEM images of NH_2-MIL-125 synthesized with different CTAB/NH_2-BDC molar ratios. It had already been proved that the morphology of NH_2-MIL-125 was smooth circular plate when there was no CTAB used. The rest of the three samples synthesized at different CTAB/NH_2-BDC molar ratios of 0.5 (B), 1.0 (C), and 2.0 (D) basically maintained the circular plate morphology with many rough defect and pores on the surface and internal. Meanwhile, there exists a little decrease of the crystal size from 700 nm to around 500 nm. A large number of voids are observed in the interior of NH_2-MIL-125 synthesized with CTAB through the TEM images and apparently the amount of voids is larger at a higher CTAB/NH_2-BDC molar ratio.

XRD patterns of the four samples are shown in Fig. 2. It can be seen from Fig. 2(A) that the corresponding XRD pattern clearly suggests that the addition of CTAB does not affect the topology and the crystallinity of NH_2-MIL-125.

The thermal behavior of these four samples was tested by TG measurement (Fig. 3). All TG/DTG curves show a mainly two-step weight loss. The first weight loss from 45 to 100 °C is the departure of the guest molecules adsorbed in the pores. The main weight loss, between 300 and 600 °C, corresponds to a series of processes of the degradation of the MOFs framework and the decomposition of the aminoterephthalic acid from the framework, finally producing amorphous TiO_2 residue. As the products have already been calcined at 200 °C for 6 hours to remove CTAB before TG measurement, there is no new weight loss observed when comparing CTAB assisted synthesized materials with sample A.

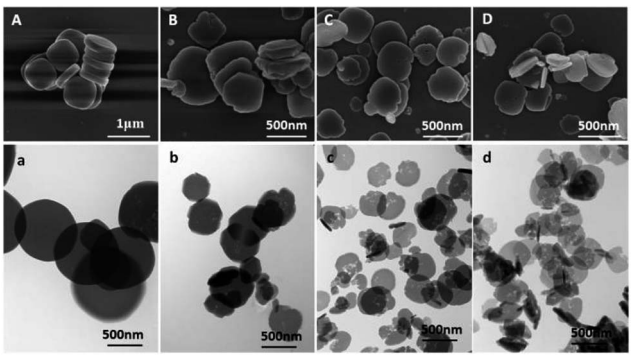

Fig. 1 SEM (A–D) and TEM (a–d) images of NH_2-MIL-125 synthesized with CTAB (CTAB/NH_2-BDC molar ratios: (A) 0; (B) 0.5; (C) 1.0; (D) 2.0; (a–d) TEM images of A–D).

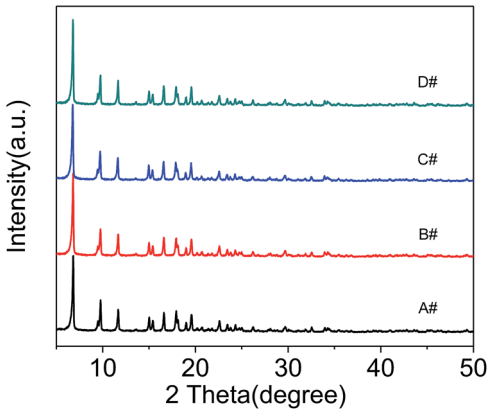

Fig. 2 XRD spectra of NH_2-MIL-125 synthesized with CTAB (CTAB/NH_2-BDC molar ratios: (A) 0; (B) 0.5; (C) 1.0; (D) 2.0).

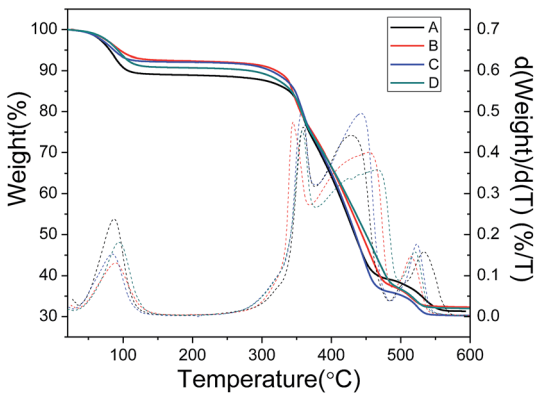

Fig. 3 TG/DTG curves of NH_2-MIL-125 synthesized with CTAB (CTAB/NH_2-BDC molar ratios: (A) 0; (B) 0.5; (C) 1.0; (D) 2.0).

Fig. 4 shows the Ar adsorption and desorption isotherms at 87 K and the pore size distributions. The Ar adsorption and desorption isotherms of all these four samples show a typical type I (micropore) characteristics. It is found that samples synthesized with CTAB show further Ar uptake at high p/p_0 (0.9–1.0) which demonstrates the existence of macropores. The pore distribution of the CTAB assisted synthesized samples altered from a micropore system to a hierarchical pore system with a wide-range mesopore and macropore distribution from 10 nm to 100 nm. The calculated specific surface area, total pore volume and micropore volume were listed in Table 1 to make a detailed comparison of the pore volume, and we calculated the ratio of micropore volume to the total pore volume which could indicate the volume of mesopore and macropore. It shows a little decrease in the specific surface area and micropore volume with the increased amount of CTAB, while the total pore volume irregularly increased a little. The decrease of V_{micro}/V_{total} ratios shows the raise of mesopore and macropore of the sample which is attributed to the addition of CTAB.

NH_2-MIL-125(Ti), containing NH_2-BDC units as the organic linkers, is known as a visible-light-absorbing MOF. The light response property was analyzed by UV/Vis spectroscopy. Fig. 5 shows the UV/vis diffuse reflectance spectra of the as-prepared

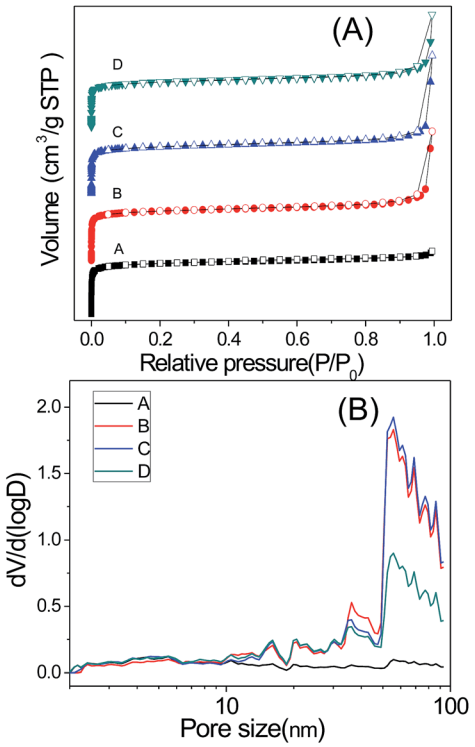

Fig. 4 Ar adsorption and desorption isotherms at 87 K and pore size distributions of NH_2-MIL-125 synthesized with CTAB. The pore size distributions were determined by non-local density functional theory (NLDFT) (CTAB/NH_2-BDC molar ratios: (A) 0; (B) 0.5; (C) 1.0; (D) 2.0).

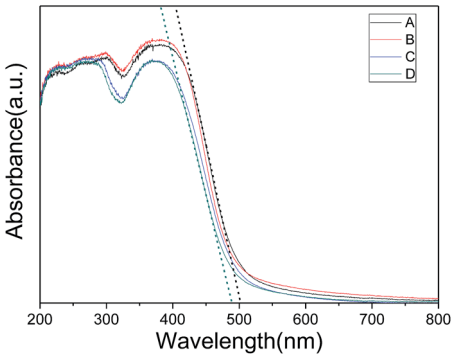

Fig. 5 UV/vis diffuse reflectance spectra of NH_2-MIL-125 synthesized with CTAB (CTAB/NH_2-BDC molar ratios: (A) 0; (B) 0.5; (C) 1.0; (D) 2.0).

samples. It can be found that the three samples synthesized with different amount of CTAB show similar absorption spectra as original NH_2-MIL-125. However, there exists slight blue shift of absorption edge for the CTAB assisted samples. Even so, all the four samples show good optical adsorption in visible light region which makes them promising photocatalysts.

Photocatalytic performance

To determine the photocatalytic activity of the as-prepared samples, the degradation of organic dye (RhB) was selected as the model photocatalytic reactions. The specific reaction conditions are relatively rigorous compared with the literatures. In specific, 20 mg catalyst was used to degrade 50 mL RhB aqueous solution (100 mg L^{-1}). For comparison, the commercial photocatalyst P25 was also tested under the same conditions, as shown in Fig. 6. It can be seen that there is no removal of RhB in the absence of photocatalyst or using P25 as the catalyst under the same experimental conditions whereas all the as-prepared NH_2-MIL-125 show high removal efficiency (Fig. 6). The dyes removal is the conjugation of adsorption and photodegradation. As shown in Fig. 6(a), the removal of RhB owing to the adsorption was raised from 9% (sample A) to 37% (sample D) while the total removal of RhB was raised from 45% (sample A) to 84% (sample D). To be specific, the adsorption and photocatalysis degradation per surface area were measured as listed in Table 2. It can be seen that both the adsorption and degradation capabilities increased from A to D, especially the adsorption/S_{BET} raised from 0.007 to 0.024. The high adsorption capability can be attributed to the hierarchical pore system formed in NH_2-MIL-125. The obtained CTAB-assisted synthesized NH_2-MIL-125 has a wide-range mesopore and macropore distribution from 10 nm to 100 nm which is beneficial for the adsorption of RhB. The adsorption capacity of RhB increased with the raise of mesopore and macropore volume.

To achieve a better understanding of the reaction kinetics of the RhB degradation catalyzed by the as-prepared NH_2-MIL-125 photocatalysts, the kinetic curves for RhB photodegradation were plotted according to the pseudo-first order model ($\ln(C_0/C) = kt$) as is shown in Fig. 6(b). The values of rate constant (k) can be calculated from the slope and the intercept of the linear plot (Fig. 6(c)). The order of RhB degradation rate for these four samples is D (0.01154 min^{-1}) > C (0.00864 min^{-1}) > B (0.00678 min^{-1}) > A (0.00428 min^{-1}). It is noteworthy that with the increase of CTAB added, the photocatalytic activity of NH_2-MIL-125 shows a rise from 0.00428 min^{-1} (sample A) to 0.01154 min^{-1} (sample D). The increase of photodegradation activity is owed to a comprehensive effect of the enrichment of RhB and the promoted diffusion of RhB and the decomposition product

Table 1 Sorption data of NH_2-MIL-125(Ti) samples

Sample	S_{BET}[a] (m^2 g^{-1})	V_{total}[b] (cm^3 g^{-1})	V_{micro}[c] (cm^3 g^{-1})	V_{meso} (cm^3 g^{-1})	V_{micro}/V_{total}
A	1298	0.55	0.48	0.07	0.87
B	1258	0.60	0.46	0.14	0.78
C	1186	0.58	0.44	0.14	0.76
D	1133	0.55	0.42	0.13	0.76

[a] Surface area calculated by using the BET model. [b] Pore size distribution and total pore volume calculated by using the NLDFT model. [c] Micropore volume calculated by using the SF model.

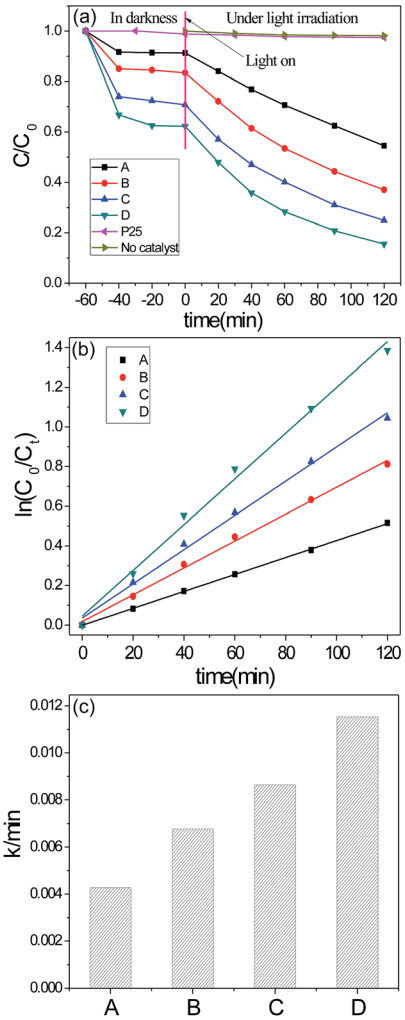

Fig. 6 (a) RhB photocatalytic degradation performance of NH_2-MIL-125. For comparison, none catalyst and P25 are also tested. (b) Kinetic curves for RhB photodegradation following pseudo-first order model ($\ln(C_0/C) = kt$). In this function C_0 is the concentration of RhB at T = 0 min. (c) The rate constant k of NH_2-MIL-125.

Table 2 Adsorption and photocatalysis degradation of RhB per surface area

Sample	S_{BET} ($m^2\ g^{-1}$)	Adsorption (%)/S_{BET} ($m^2\ g^{-1}$)	Degradation (%)/S_{BET} ($m^2\ g^{-1}$)
A	1298	0.007	0.029
B	1258	0.014	0.037
C	1186	0.024	0.039
D	1133	0.034	0.041

which both benefit from the hierarchical pores formed in the sample of CTAB assisted NH_2-MIL-125. Meanwhile, the blue shift of absorption edge for the CTAB assisted samples analyzed by UV/Vis spectroscopy may lead to an enhancement of the absorption of visible light and increase the photocatalytic activity. This proves to be an effective method to improve the dye removal capacity by using hierarchical NH_2-MIL-125.

Recyclability and stability of catalyst

The recycle experiments of the CTAB assisted synthesized NH_2-MIL-125 with the best RhB removal (sample D) were evaluated under the same conditions to study the stability of the photocatalyst. Fig. 7 shows the results of the photodegradation of RhB after 4th-runs. The catalyst shows a little decrease of adsorption capacity and photodegradation efficiency and the RhB removal dropped from 84% to 73% which indicates that the catalyst can be used successively without obvious variation of photocatalytic performance. XRD patterns (Fig. 7(c)) of fresh and used catalyst (used fourth time) proves the stability of NH_2-MIL-125 after 4th-runs. Therefore, NH_2-MIL-125 using CTAB as additives to form hierarchical structures shows promising applications in wastewater treatment.

Photocatalytic performance of hierarchical NH_2-MIL-125 with different morphologies

A series of hierarchical NH_2-MIL-125 with different morphologies were synthesized through a similar CTAB assisted method combining the morphology-controlled strategy of our previous work.[22] Specifically, hierarchical NH_2-MIL-125 with

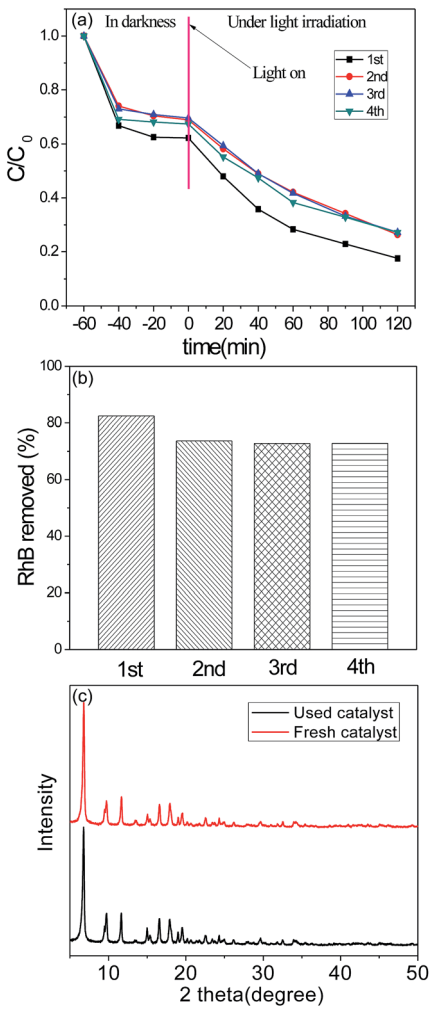

Fig. 7 (a) Recyclability of sample D. (b) The removal of RhB. (c) XRD patterns of fresh and used catalyst.

controllable morphologies from tetragonal plate to truncated bipyramid and octahedron were obtained using CTAB as additives. The SEM and TEM images show that the morphologies were basically maintained when compared with the original microporous NH_2-MIL-125, only with many rough defects and pores on the surface and internal (Fig. 8). The obtained hierarchical NH_2-MIL-125 and the original microporous NH_2-MIL-125 with controllable morphologies were applied to the photodegradation of RhB, and the performance was compared in Fig. 9. The four hierarchical NH_2-MIL-125 samples with different morphologies show a raised RhB removal from about 50% (microporous NH_2-MIL-125) to approximately 80% (hierarchical NH_2-MIL-125) owing to the increase of adsorption and the enhancement of photocatalytic activity. It could be believed that the CTAB assisted synthetic strategy is suitable for more systems to obtain hierarchical MOFs.

Conclusions

In summary, we showed a simple solvothermal method to synthesize NH_2-MIL-125 with substantial hierarchical pores by employing surfactant CTAB as an additive. The obtained visible-light photocatalyst NH_2-MIL-125 showed a great increase of the removal of organic pollutants due to the produced hierarchical pores through the use of surfactant. On one hand the increased porosity improved the adsorption capacity of RhB, and on the other hand it could benefit the diffusion of decomposed pollutants during the photodegradation under visible-light irradiation. The adsorption removal of RhB increased 28% on hierarchical NH_2-MIL-125. Meanwhile, the photodegradation rate of RhB increased 2.4 times according to the structure with abundant mesopores and macropores. Considering these two process, the total removal of RhB doubled due to the hierarchical structure of NH_2-MIL-125. Cyclic experiments also indicated the stability and reusability of the catalyst for RhB removal. Furthermore, hierarchical NH_2-MIL-125 with different morphologies were prepared using the same CTAB assisted method and obtained an enhanced removal of organic pollutant. Since the properties of MOFs can be readily tuned by varying the constituent metal ions and bridging organic linkers, it is promising to extend this strategy to other MOFs-based photocatalysts for the applications of environmental remediation.

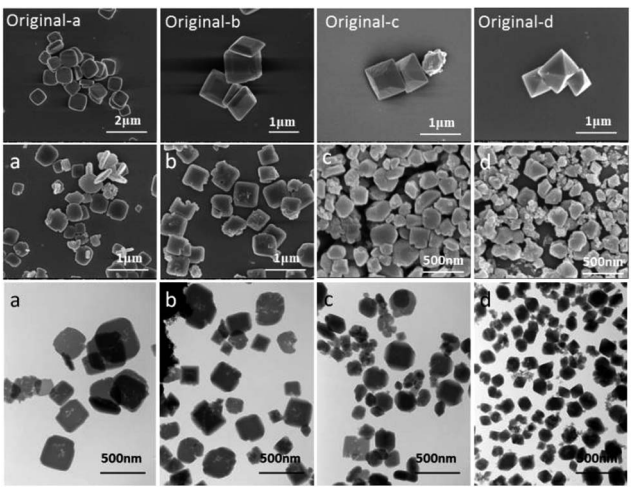

Fig. 8 SEM and TEM images of NH_2-MIL-125 with different morphologies (original-a to original-d: SEM images of microporous NH_2-MIL-125 with different morphologies; (a–d) SEM and TEM images of hierarchical NH_2-MIL-125 with different morphologies).

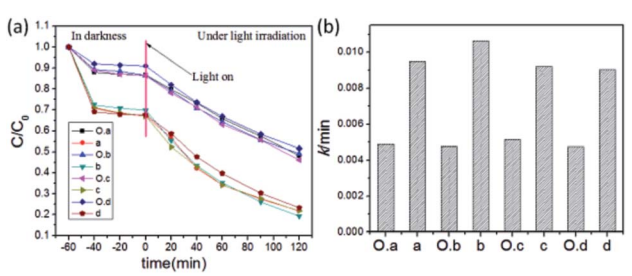

Fig. 9 RhB photocatalytic degradation performance of NH_2-MIL-125.

Acknowledgements

This work was supported by the State Key Program of the National Natural Science Foundation of China (Grant No. 21236008, 21401017).

Notes and references

1 (*a*) G. M. Zeng, M. Chen and Z. T. Zeng, *Science*, 2013, **340**, 1403; (*b*) B. Petrie, R. Barden and B. Kasprzyk-Hordern, *Water Res.*, 2015, **72**, 3–27.

2 (*a*) N. Bolong, A. F. Ismail, M. R. Salim and T. Matsuura, *Desalination*, 2009, **239**, 229–246; (*b*) D. Rajkumar and K. Palanivelu, *J. Hazard. Mater.*, 2004, **113**, 123–129; (*c*) K. Kabra, R. Chaudhary and R. L. Sawhney, *Ind. Eng. Chem. Res.*, 2004, **43**, 7683–7696.

3 (*a*) V. K. Gupta and Suhas, *J. Environ. Manage.*, 2009, **90**, 2313–2342; (*b*) G. Crini, *Bioresour. Technol.*, 2006, **97**, 1061–1085; (*c*) M. R. Hoffmann, S. T. Martin, W. Choi and D. W. Bahnemann, *Chem. Rev.*, 1995, **95**, 69–96; (*d*) J. M. Herrmann, *Catal. Today*, 1999, **53**, 115–129.

4 (*a*) A. Wang, Y. Zhou, Z. Wang, M. Chen, L. Sun and X. Liu, *RSC Adv.*, 2016, **6**, 3671–3679; (*b*) H. Wang, X. Yuan, Y. Wu, G. Zeng, H. Dong, X. Chen, L. Leng, Z. Wu and L. Peng, *Appl. Catal., B*, 2016, **186**, 19–29; (*c*) X. Wu, S. Yin, D. Xue, S. Komarneni and T. Sato, *Nanoscale*, 2015, **7**, 17048–17054.

5 (*a*) O. M. Yaghi, M. O'Keeffe, N. W. Ockwig, H. K. Chae, M. Eddaoudi and J. Kim, *Nature*, 2003, **423**, 705; (*b*) N. Stock and S. Biswas, *Chem. Rev.*, 2012, **112**, 933–969; (*c*) N. C. Burtch, H. Jasuja and K. S. Walton, *Chem. Rev.*, 2014, **114**, 10575–10612; (*d*) E. Barea, C. Montoro and J. A. Navarro, *Chem. Soc. Rev.*, 2014, **43**, 5419–5430; (*e*) S. Qiu, M. Xue and G. Zhu, *Chem. Soc. Rev.*, 2014, **43**, 6116–6140; (*f*) A. Corma, H. Garcıía and F. X. Llabrés i Xamena, *Chem. Rev.*, 2010, **110**, 4606–4655; (*g*) J. Park, Q. Jiang,

D. Feng, L. Mao and H. C. Zhou, *J. Am. Chem. Soc.*, 2016, **38**, 3518–3525; (*h*) S. Krause, V. Bon, I. Senkovska, U. Stoeck, D. Wallacher, D. M. Tobbens, S. Zander, R. S. Pillai, G. Maurin, F. X. Coudert and S. Kaskel, *Nature*, 2016, **532**, 348–352; (*i*) D. A. Gomez and G. Sastre, *Phys. Chem. Chem. Phys.*, 2011, **13**, 16558–16568; (*j*) D. A. Gomez, J. Toda and G. Sastre, *Phys. Chem. Chem. Phys.*, 2014, **16**, 19001–19010.

6 (*a*) X. Wang and A. J. Jacobson, *Microporous Mesoporous Mater.*, 2016, **219**, 112–116; (*b*) Z. P. Qi, J. M. Yang, Y. S. Kang, F. Guo and W. Y. Sun, *Dalton Trans.*, 2016, **45**, 8753–8759; (*c*) F. Tan, M. Liu, K. Li, Y. Wang, J. Wang, X. Guo, G. Zhang and C. Song, *Chem. Eng. J.*, 2015, **281**, 360–367.

7 (*a*) G. Palmisano, V. Augugliaro, M. Pagliaro and L. Palmisano, *Chem. Commun.*, 2007, 3425–3437; (*b*) D. Ravelli, D. Dondi, M. Fagnoni and A. Albini, *Chem. Soc. Rev.*, 2009, **38**, 1999–2011; (*c*) T. Zhang and W. Lin, *Chem. Soc. Rev.*, 2014, **43**, 5982–5993; (*d*) C.-C. Wang, J.-R. Li, X.-L. Lv, Y.-Q. Zhang and G. Guo, *Energy Environ. Sci.*, 2014, **7**, 2831.

8 (*a*) K. G. Laurier, F. Vermoortele, R. Ameloot, D. E. De Vos, J. Hofkens and M. B. Roeffaers, *J. Am. Chem. Soc.*, 2013, **135**, 14488–14491; (*b*) Q. Sun, M. Liu, K. Li, Y. Han, Y. Zuo, J. Wang, C. Song, G. Zhang and X. Guo, *Dalton Trans.*, 2016, **45**, 7952–7959.

9 C.-N. Lü, M.-M. Chen, W.-H. Zhang, D.-X. Li, M. Dai and J.-P. Lang, *CrystEngComm*, 2015, **17**, 1935–1943.

10 A. Abbasi, M. Soleimani, M. Najafi and S. Geranmayeh, *Inorg. Chim. Acta*, 2016, **439**, 18–23.

11 (*a*) M. Dan-Hardi, C. Serre, T. Frot, L. Rozes, G. Maurin, C. Sanchez and G. Ferey, *J. Am. Chem. Soc.*, 2009, **131**, 10857–10859; (*b*) Y. Fu, D. Sun, Y. Chen, R. Huang, Z. Ding, X. Fu and Z. Li, *Angew. Chem., Int. Ed. Engl.*, 2012, **51**, 3364–3367.

12 Y. Fu, L. Sun, H. Yang, L. Xu, F. Zhang and W. Zhu, *Appl. Catal., B*, 2016, **187**, 212–217.

13 (*a*) H. Wang, X. Yuan, Y. Wu, G. Zeng, X. Chen, L. Leng and H. Li, *Appl. Catal., B*, 2015, **174–175**, 445–454; (*b*) L. Huang and B. Liu, *RSC Adv.*, 2016, **6**, 17873–17879.

14 R. N. Amador, M. Carboni and D. Meyer, *Mater. Lett.*, 2015, **167**, 188–191.

15 (*a*) L. Peng, J. Zhang, J. Li, B. Han, Z. Xue and G. Yang, *Chem. Commun.*, 2012, **48**, 8688–8690; (*b*) Y. Zhao, J. Zhang, B. Han, J. Song, J. Li and Q. Wang, *Angew. Chem., Int. Ed. Engl.*, 2011, **50**, 636–639; (*c*) Z. Zhang, Y. Chen, S. He, J. Zhang, X. Xu, Y. Yang, F. Nosheen, F. Saleem, W. He and X. Wang, *Angew. Chem., Int. Ed. Engl.*, 2014, **53**, 12517–12521; (*d*) A. Ahmed, M. Forster, R. Clowes, P. Myers and H. Zhang, *Chem. Commun.*, 2014, **50**, 14314–14316; (*e*) H. Huang, J. R. Li, K. Wang, T. Han, M. Tong, L. Li, Y. Xie, Q. Yang, D. Liu and C. Zhong, *Nat. Commun.*, 2015, **6**, 8847; (*f*) Y. Yue, P. F. Fulvio and S. Dai, *Acc. Chem. Res.*, 2015, **48**, 3044–3052.

16 N. D. McNamara and J. C. Hicks, *ACS Appl. Mater. Interfaces*, 2015, **7**, 5338–5346.

17 (*a*) Y. F. Lu, R. Ganguli, C. A. Drewien, M. T. Anderson, C. J. Brinker, W. L. Gong, M. H. Huang and J. I. Zink, *Nature*, 1997, **389**, 364–368; (*b*) Z. R. Tian, W. Tong, J. Y. Wang, N. G. Duan, V. V. Krishnan and S. L. Suib, *Science*, 1997, **276**, 926–930; (*c*) A. Walcarius, E. Sibottier, M. Etienne and J. Ghanbaja, *Nat. Mater.*, 2007, **6**, 602–608; (*d*) M. B. Yue, W. Q. Jiao, Y. M. Wang and M.-Y. He, *Microporous Mesoporous Mater.*, 2010, **132**, 226–231.

18 (*a*) Y. H. Deng, D. W. Qi, C. H. Deng, X. M. Zhang and D. Y. Zhao, *J. Am. Chem. Soc.*, 2008, **130**, 28–29; (*b*) J. Y. Kim, J. E. Lee, J. W. lee, J. H. Yu, B. C. Kim, K. An, Y. Hwang, C. H. Shin, J. G. Park, J. Kim and T. Hyeon, *J. Am. Chem. Soc.*, 2006, **128**, 688–689.

19 Z. T. Zhang, Y. Han, L. Zhu, R. W. Wang, Y. Yu, S. L. Qiu, D. Y. Zhao and F. X. Xiao, *Angew. Chem., Int. Ed.*, 2001, **40**, 1258–1262.

20 (*a*) S. Besson, T. Gacoin, C. Ricolleau, C. Jacquiod and J.-P. Boilot, *J. Mater. Chem.*, 2003, **13**, 404–409; (*b*) S. Besson, C. Ricolleau, T. Gacoin, C. Jacquiod and J. P. Boilot, *J. Phys. Chem. B*, 2000, **104**, 12095–12097.

21 (*a*) X. L. Yan, X. Y. Hu and S. Komarneni, *RSC Adv.*, 2014, **4**, 57501–57504; (*b*) X. X. Huang, L. G. Qiu, W. Zhang, Y. P. Yuan, X. Jiang, A. J. Xie, Y. H. Shen and J. F. Zhu, *CrystEngComm*, 2012, **14**, 1613–1617.

22 S. Hu, M. Liu, K. Li, Y. Zuo, A. Zhang, C. Song, G. Zhang and X. Guo, *CrystEngComm*, 2014, **16**, 9645–9650.